Title

6000 lines/mm blazed grating for a high-resolution x-ray spectrometer.

Journal

Optics Express, 30(16)

ISSN

1094-4087

Authors

Voronov, DL

Park, S

Gullikson, EM

et al.

Publication Date

2022-08-01

DOI

10.1364/oe.460740

Research Article | Vol. 30, No. 16 / 1 Aug 2022 / Optics Express 28783
Optics EXPRESS

6000 lines/mm blazed grating for a high-resolution x-ray spectrometer

D. L. VORONOV,* S. PARK, E. M. GULLIKSON, F. SALMASSI, AND H. A. PADMORE

Lawrence Berkeley National Laboratory, 1 Cyclotron Road, Berkeley, California 94720, USA
**dlvoronov@lbl.gov*

Abstract: We have designed and fabricated a high groove density blazed grating for a Resonant Inelastic X-ray Scattering spectrometer for the new Qerlin beamline at the Advanced Light Source (ALS) synchrotron facility. The gratings were fabricated using a set of nanofabrication techniques including e-beam lithography, nanoimprint, plasma etch, and anisotropic wet etching. Two gratings with groove density of 6000 lines/mm and 3000 lines/mm and optimized for operation in the 1st and 2nd negative diffraction order respectively were fabricated and tested. We report on fabrication details and characterization of the gratings at beamline 6.3.2 of the ALS.

1. Introduction

Resonant Inelastic X-ray Scattering (RIXS) is a powerful tool for investigation of the electron structure of solids and is crucial for research on energy-related materials and their chemical functionalities, as well as on quantum materials with strong electronic correlations [1]. Since the RIXS process is free of life-time related energy broadening, it is intrinsically a high-resolution technique which is capable of probing the very low energy electron excitations in solids which lead to exotic properties such as superconductivity. To achieve the very high resolving power that RIXS is capable of and is needed for probing low energy excitations in solids, either very large spectrometers are required (> 10 m grating to detector distance) [2,3] or diffraction gratings with very high groove density are needed, or a combination of the two. At the same time, high diffraction efficiency is needed for this type of spectroscopy due to the low cross section of the scattering process and the limited solid angle that can be collected by x-ray optics. These are however conflicting requirements since the high dispersion of a high groove density grating inevitably drives the grazing angles of incidence and diffraction to large values and consequently this reduces the diffraction efficiency of the grating.

Although lamellar gratings are easier to make, they have significantly lower diffraction efficiency especially for high diffraction orders. Blazed gratings have at least twice the efficiency of lamellar gratings [4] even in a high diffraction order. This makes them attractive for high resolution applications such as RIXS, where the signal can be very weak and so the highest spectrometer efficiency is extremely important. They are however much more challenging to make. The fabrication process should provide a perfect triangular groove shape and nanometer-scale accuracy for the groove placement. Any imperfections of the groove profile would cause an efficiency drop while errors in groove position would affect the imaging properties of the grating and compromise the spectral resolution of a spectrometer. The requirements are extremely challenging to meet with mechanical ruling, a primary method for producing blazed gratings [5,6]. Alternatively, the gratings can be made using a set of nanofabrication techniques based on beam e-beam lithography (EBL) and anisotropic etching of Si single crystals [7,8] which provides both nanometer placement accuracy and a near-perfect groove shape. We have investigated various aspects of this approach earlier and demonstrated fabrication of high-quality test gratings with groove density up to 10,000 lines/mm [9–13]. In this paper we report for the first time on

#460740 https://doi.org/10.1364/OE.460740
Journal © 2022 Received 7 Apr 2022; revised 10 Jun 2022; accepted 12 Jun 2022; published 21 Jul 2022

Optics EXPRESS

the fabrication of full-sized blazed gratings with a groove density of 6000 lines/mm on x-ray quality substrates for ultra-high resolution soft x-ray spectroscopy.

2. Blazed VLS grating design and optimization

The gratings are to be installed in the RIXS spectrometer of the Qerlin beamline which is currently under construction at the Advanced Light Source (ALS). The design of the unique cross dispersion spectrometer was published earlier [14]. In a regular RIXS measurement, monochromatic photons are focused on a sample, and scattered photons of different energies are dispersed and focused to different positions on a detector. This measurement is then repeated for many incident photon energies through a core level absorption edge. The RIXS map of photon energy out versus photon energy in is therefore accumulated spectrum by spectrum in a serial manner. The double dispersion geometry of the Qerlin spectrometer results in a RIXS map being collected in parallel, therefore increasing spectrometer throughput, which is critical in these photon hungry experiments. The imaging plane of the spectrometer produces a 2D field of incident photon energy versus scattered photon energy. The layout of this 4.5-meter-long spectrometer is depicted in Fig. 1.

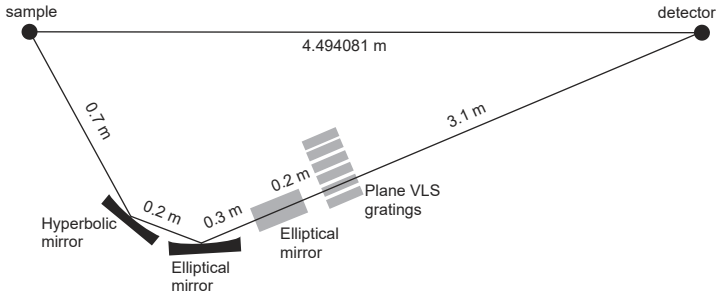

Fig. 1. A layout of the 4.5 meter long RIXS spectrometer of the ALS Qerlin beamline.

The beamline illuminates a vertical stripe on the sample with incident photon energies dispersed across its surface in the vertical direction, which is a source for the cross-dispersion RIXS spectrometer. A Wolter I type objective composed of hyperbolic and elliptical mirrors provides flat field imaging of the stripe on the detector in the vertical plane. A high-resolution grating system disperses and images the scattered photons in the orthogonal plane.

The optical scheme of the spectrometer in the dispersion plane is shown in Fig. 2. This is a Hettrick-Underwood design [15] which provides an erect focal plane required for the two-dimensional imaging in which an elliptical mirror provides perfect imaging of a point source. The image serves as a virtual source for the Varied Line Spacing (VLS) grating and is located at a distance r_A = - 3.08818 m behind the grating. The grating provides focusing of the divergent beam at the detector located at a distance of r_B = 3.1 m from the grating.

In this scheme the grating does not rotate. A wide energy range of operation of the spectrometer is achieved by using a set of diffraction gratings, each optimized for a specific absorption edge. The gratings are moved into the x-ray beam on a linear translator. To achieve the required high resolving power of 30,000 the gratings must have a high groove density and / or operate in a high diffraction order. For example, a 5000 lines/mm grating operating in 1st negative order is needed for RIXS measurements around an energy of 710 eV for the iron L_3 edge. For the central point of the grating the angles of incidence and diffraction are $\alpha = 82°$ and $\beta = - 87.2858°$ respectively.

Incidence and diffraction angles are the same for all the gratings while the groove density is scaled accordingly to match energy for a specific absorption edge. For example, a 1st order grating for energy of 850 eV for the Ni L_3 edge should have a central groove density g_0 = 5902.78

Optics EXPRESS

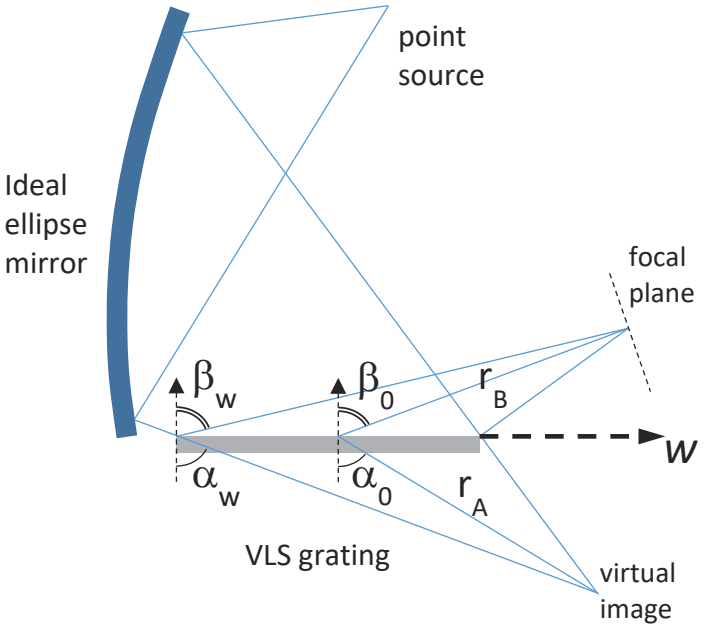

Fig. 2. Schematic of the Qerlin spectrometer in the dispersion plane.

lines/mm. The groove density can be reduced by a factor of two down to $g_0 = 2951.39$ lines/mm for blazed grating operating in the 2nd negative order. In the following, we will refer to the groove density of the 1st and 2nd order gratings as 6000 lines/mm and 3000 lines/mm respectively for the sake of simplicity.

To provide aberration-free focusing of the illuminated area of the sample at the detector in the dispersion plane, the groove density of a grating should vary along the grating length in a certain way usually expressed in a polynomial form:

$$g(w) = g_o + g_1 w + \ldots + g_k w^k \tag{1}$$

The linear term $g_1 = 3.80397\ \mathrm{mm}^{-2}$ can be found using the focusing condition for the erect focal plane:

$$\frac{cos^2\alpha}{r_A} + \frac{cos^2\beta}{r_B} = m\lambda g_1 \tag{2}$$

where r_A and r_B are the sample to grating and grating to focal plane distances. The 2nd order g_2 term can also be found analytically, but as we need to find higher polynomial terms for adequate imaging quality, these are found using ray tracing assuming ideal point-to-point imaging of the imaginary source. The local groove density, $g(w)$, for any point along the grating length, w, can be found from the local incidence and diffraction angles using the grating equation:

$$g(w) = (\sin\alpha_w - \sin\beta_w)/m\lambda \tag{3}$$

The ideal varied groove density can be approximated by a polynomial series (Eq. (1)). For example, polynomial coefficients calculated by up to the 4th order fitting for the 1st and 2nd order gratings are listed in Table 1.

We found that inclusion of the 3rd and 4th order polynomial terms are unnecessary for adequate imaging quality. The residual displacement of the grooves from their ideal positions is significantly below the typical grid size of 1 nm (Fig. 3(a)) for the e-beam lithography process.

Optics EXPRESS

Table 1. VLS parameter for the 1st and 2nd order diffraction gratings

VLS coefficients	1st order grating	2nd order grating
g_0, mm^{-1}	5902.78	2951.39
g_1, mm^{-2}	3.80397	1.901985
g_2, mm^{-3}	0.00183	0.000916
g_3, mm^{-4}	7.7699×10^{-7}	3.88495×10^{-7}
g_4, mm^{-5}	3.07787×10^{-10}	1.538935×10^{-10}

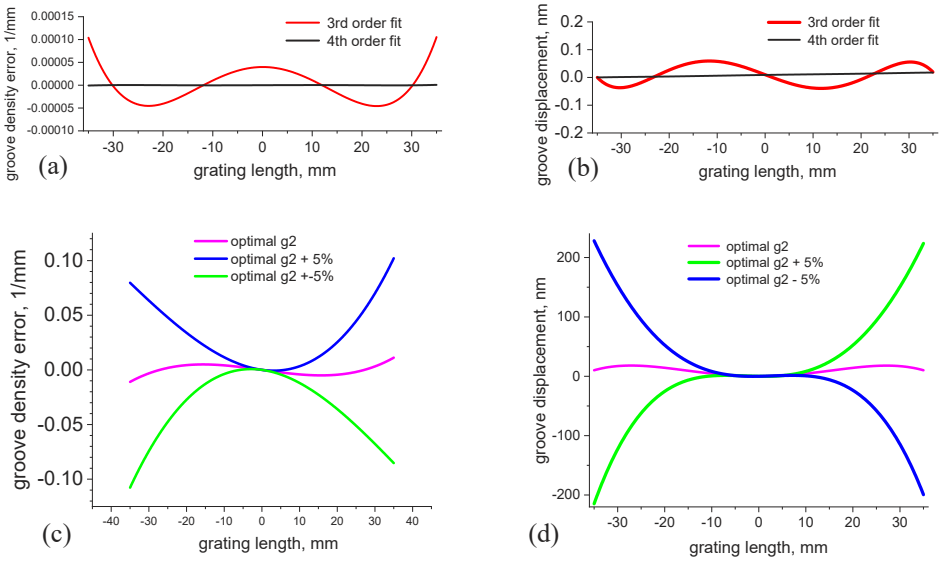

Fig. 3. Residual groove density errors (a) and groove displacement (b) for 3rd and 4th order fitting of the ideal groove density; (c), (d) the same for the 2nd order fit using an optimal g_2 and for +/- 5% error in g_2.

The 2nd order fitting results in residual errors of 10^{-2} lines/mm for the groove density (Fig. 3(b)) and groove displacement up to +/- 10 nm (Fig. 3(c)). The impact of the groove displacement on the resolving power of the spectrometer can be evaluated by ray tracing. Figure 4(a) shows images of a point source at the detector plane, simulated for three different energies corresponding to a resolving power of R = 30,000. The 3rd and 4th order groove density fitting provides perfect focusing into three lines separated by 20 µm which exceeds by a factor of 4 the pixel size of 5 µm of the detector. The exact 2nd order parameter results in insignificant blurring of the spectral lines when considering in comparison the effect of the finite source size; this is shown in Fig. 4(c) for the real source size of 2.2 µm FWHM. However, the tolerance for the g_2 coefficient is very tight. Deviation from the optimal g_2 value by +/- 5% results in groove density errors of 0.1 lines/mm and groove displacement up to 200 nm (Figs. 3(b) and 3(c)). This would cause a significant blurring of the image of the point source (Figs. 4(e) and 4(f)) and compromise the resolving power. Note, even the 5% precision is extremely challenging to achieve for traditional grating fabrication techniques. For example, for holographically recorded gratings a g_2 error of 15% at best is typically achieved.

To generate the grating pattern, the position of every groove, x_n, was calculated using a recursive formula and the g_n coefficients listed in Table 1

$$x_n = x_{n-1} + 1/(g_o + g_1 x_{n-1} + \ldots + g_4 x_{n-1}^4) \tag{4}$$

Optics EXPRESS

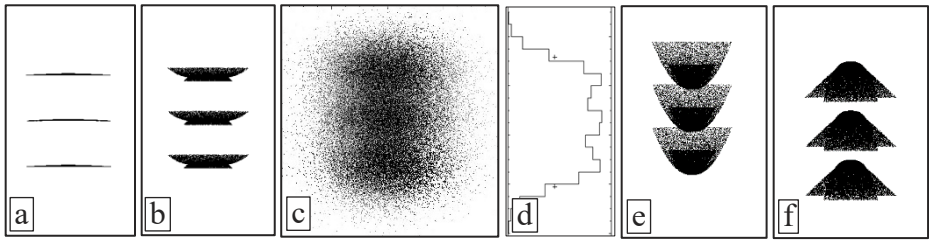

Fig. 4. Ray tracing images at the detector plane simulated for energy of 850 eV and 850 +/- 0.028 eV for a point source (a), (b), (e), (f) and the real size source of 2.2 µm (c). The lines are separated by a distance of 20 µm. The images were simulated for the VLS groove density obtained by 4th order (a),(c) and 2nd order fits using an optimal g_2 (b) and for +/- 5% deviation from the optimal g_2 (e), (f). A histogram for the image of the real size source and 5-micron pixel size (d).

where n is a number of a groove, for $-35\ mm \le x \le 35mm$ and $x_0 = 0$ for the groove in the center of the 70 mm long grating pattern.

To provide the maximum possible efficiency the grating grooves should have a saw-tooth shape. This is especially crucial for operation in the 2nd diffraction order.

Optimal blaze angles for 1st and 2nd order gratings were found via efficiency simulations using PCGrate 6.5 software which uses the integral formalism of the electromagnetic theory of gratings [16]. The absolute efficiency was calculated for gold gratings with ideal triangular grooves with an anti-blaze angle of 20° and different blaze angles in the range from 0.7° to 5.4° at an angle of incidence of 82° for an energy of 850 eV. An optimal blaze angle of 2.9° provides the maximum efficiency for both the gratings. The simulations showed that the 1st order grating is preferable since it has a somewhat higher theoretical efficiency of 3.4% versus 3.0% for the 2nd order grating (Fig. 5). Moreover, the efficiency of the 1st order grating drops more slowly with deviation of the blaze angle from the optimal value, i.e., fabrication tolerances are more relaxed.

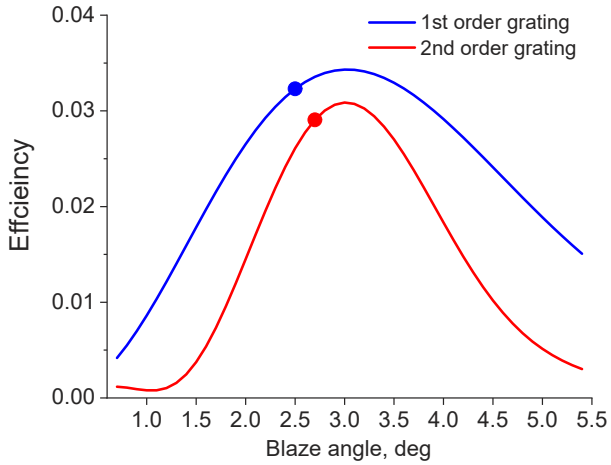

Fig. 5. Dependence of the theoretical diffraction efficiency on the blaze angle for the 1st order (blue) and 2nd (red) order gratings, simulated for a photon energy of 850 eV. The dots depict real blaze angles measured with AFM for the fabricated blazed gratings.

As was expected the theoretical diffraction efficiency of the high groove density grating is rather low and this is the price for the high grating dispersion and high resolving power of the

Optics EXPRESS

spectrometer. The simultaneous collection of the 2D RIXS map through the use of crossed dispersion is therefore critical for achieving the throughput necessary for practical experiments. The selection of a 1st or 2nd order grating is really set by the quality of grating that can be achieved. The 1st order grating has a small efficiency advantage but might be more challenging to make than the 2nd order grating. We therefore made both 1st and 2nd order gratings to compare their performance in terms of the effects of possible fabrication errors.

3. Blazed grating fabrication and characterization

The 1st and 2nd order blazed gratings were fabricated using a nanofabrication approach which provides nanometer-scale groove placement accuracy [17]. The grating patterns were recorded by commercially available e-beam lithography (EBL). High throughput variable-shaped beam EBL equipment [18] was used to reduce the writing time down to a few hours and has 10 nm absolute accuracy over a 6-inch mask. Since thick Si substrates are not compatible with commercial EBL tools the direct write approach is not possible and the patterns were recorded on standard 6" × 6" × 0.25" quartz plates and then transferred to the grating substrate surface by nanoimprinting. We used the quartz plate with the grating pattern transferred into the Cr layer on top of the plate for making a mold for the nanoimprint (Fig. 6(a)). A Reactive Ion Etch (RIE) process in a gas mixture of CHF_3 and O_2 was used to etch 150 nm deep trenches on the surface the quartz plate. The nanoimprint was applied to replicate the grating pattern into a resist layer on top of a single crystal Si grating substrate, using UV-curable resist UVCur26 from Microresist Gmbh (Fig. 6(b)). A photograph of the 90 mm × 15 mm × 19 mm single crystal substrate with the 3000 lines/mm resist pattern obtained by the nanoimprint is shown in Fig. 6(f). An RIE oxygen plasma was used to etch through the residual layer and then the resist pattern was converted into a hard mask using a lift-off process. A 20 nm thick Cr film was deposited on top of the patterned substrate and then the resist along with the Cr coating on it was removed using Piranha solution ($H_2SO_4 + H_2O_2$), leaving stripes of the Cr film deposited on the Si surface between the resist lines (Fig. 6(c)). An anisotropic wet etching using an aqueous 20% KOH solution was applied to form slanted facets of the grating grooves (Fig. 6(d)). The facet tilt angle is defined by the angle of the (111) planes of the Si single crystal with respect to the grating surface. The saw-tooth shape of the grating grooves was finalized by an isotropic etching process (Fig. 6(d)). The Si blazed grating was coated with a 30 nm thick layer of gold deposited by dc-magnetron sputtering. A 5 nm thick Cr layer was deposited prior the gold for adhesion purposes. The deposition was performed using Ar sputtering gas at the pressure of 1 mTorr.

The nanoimprint molds were inspected with SEM after the quartz plasma etch. An SEM image of the mold with the 6000 lines/mm pattern is shown in Fig. 7(a). We found that quality of the mold was not as high as expected. The lines of the pattern are quite uneven and line edge roughness (LER) is rather high (Fig. 7(a)). Also, AFM measurements revealed some variation of the groove depth. It is not clear if the imperfections were generated during the e-beam writing, resist processing, Cr etch, or quartz etch. All those steps require further verification and optimization. The mold with the 3000 lines/mm pattern exhibits much better quality of the lines and uniform groove depth (Fig. 7(b)). The mold imperfections will affect quality of the final gratings since they are transferred to the resist pattern, Cr lines, and eventually to the grating grooves.

The finished blazed gratings were inspected by AFM. To minimize impact of the tip shape on high-frequency features of the surface we used sharp silicon Otespa-R3 AFM probes from Bruker [19] with a nominal tip radius of 7 nm, and replaced them as soon as first signs of tip degradation appeared. Careful X-Y-Z calibration of the AFM scanner provided accuracy of the blaze angle measurements better than 0.1°.

Both gratings have highly smooth facets with approximately the same residual roughness below 0.4 nm rms (Fig. 8). However, much higher LER inherited from the mold is observed

Optics EXPRESS

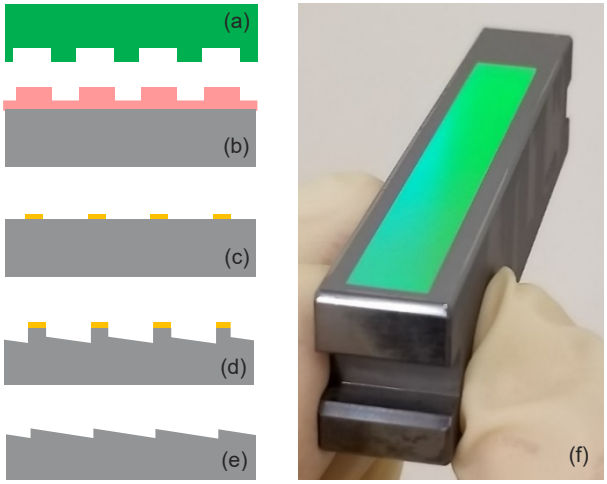

Fig. 6. Nanofabrication process flow for blazed gratings for Qeril spectrometer. Quartz mold with grating pattern made by EBL (a), Tranfer the pattern to a resist layer by nanoimprint (b), hard mask (c) for anisotropic wet etching of the single crystal Si grating substrate (d), final Si blazed grating after isotropic etching (e). The 3000 lines/mm grating patern transferred into a resist layer on top of the grating substrate (f).

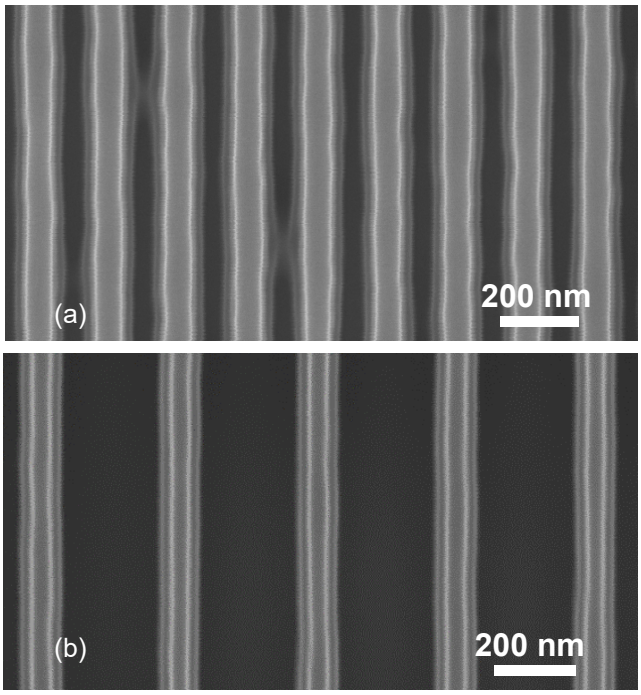

Fig. 7. SEM images of the quartz molds for the 6000 line/mm (a) and 3000 lines/mm (b) gratings.

Optics EXPRESS

for the grooves of the 1st order grating (Fig. 9). Also, the shape of the grooves was found to be substantially better for the 2nd order grating. The difference in groove profile quality for both the gratings is clearly manifested by normalized groove profiles shown in Fig. 10. The 1st order grating has significantly smoothed grooves with a low anti-blaze angle and a rounded apex of the grooves. The 2nd order grating has much a better groove profile with almost flat blazed facets, steep anti-blazed facets, and a sharp apex of the grooves.

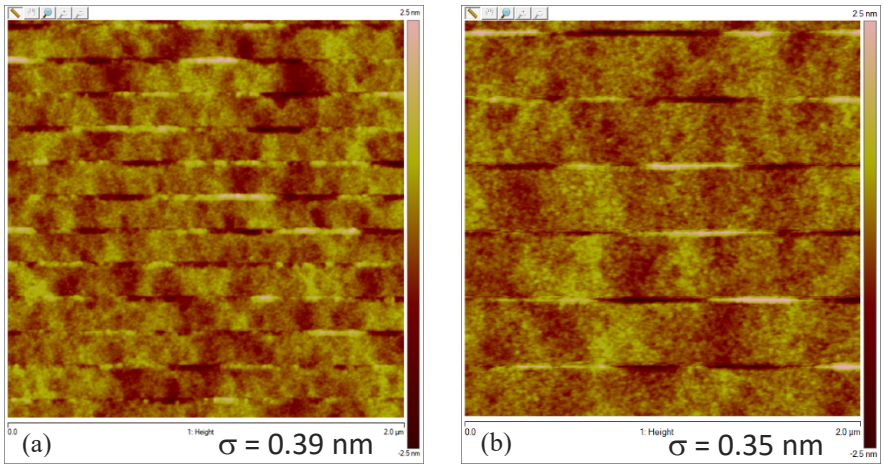

Fig. 8. AFM images of the 6000 line/mm (a) and 3000 lines/mm (b) gratings. The images were obtained by scanning along the grating grooves followed by line-by-line image planarization.

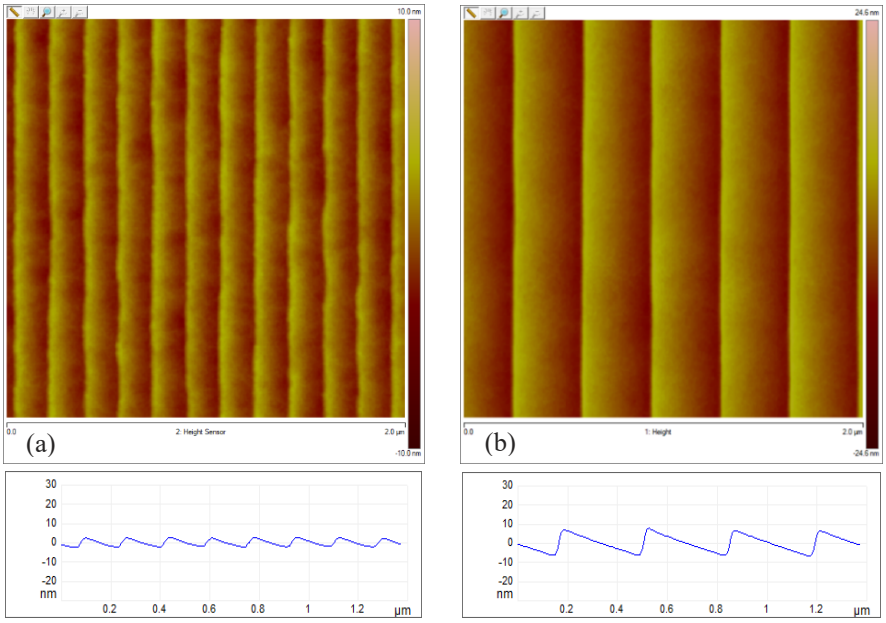

Fig. 9. AFM images and groove profiles of the 6000 line/mm (a) and 3000 lines/mm (b) gratings. The images were obtained by scanning across the grating grooves followed by line-by-line flattening. Much higher LER is observed for the 6000 line/mm grating.

Optics EXPRESS

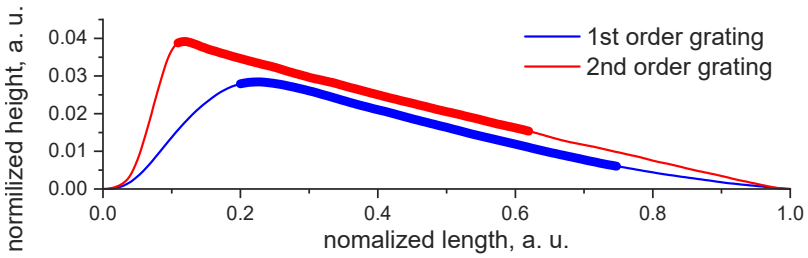

Fig. 10. Normalized AFM groove profiles of the 6000 line/mm (blue) and 3000 lines/mm (red) gratings. The lower groove density grating has much better quality of the grooves. Thick lines show the non-shadowed part of the grating facets, which contributes to the blazed order efficiency.

The blaze facets are not ideally flat and have some curvature. An effective blaze angle of the gratings can be found as an average tilt of the blazed facets using the unshadowed length of the grooves. Since the grooves of a blazed grating are partially self-shadowed only a part of the blaze facet is visible to the detector and contributes to the blazed diffraction order efficiency. The non-shadowed part AB can be found as (Fig. 11):

$$AB = \frac{AD}{AE}AC = \frac{AD}{AE}\frac{d\cos\alpha}{\cos(\alpha+\phi)} \tag{5}$$

where d is the grating period, and ϕ is the blaze angle. According to Lukirski [20] and Maystre [21] $AD/AE = \cos\beta/\cos\alpha$, and the illuminated area of the blaze facets can be calculated as:

$$AB = C_{ff}\frac{\cos\alpha}{\cos(\alpha+\phi)}d \tag{6}$$

where $C_{ff} = \cos\beta/\cos\alpha$ is a focusing constant of the grating. For the Qerlin spectrometer $\alpha = 82°$, the blaze angle is 2.9°, and C_{ff} =0.34, the non-shadowed part of the blazed facets is 0.54×d, shown in Fig. 10 by thick lines.

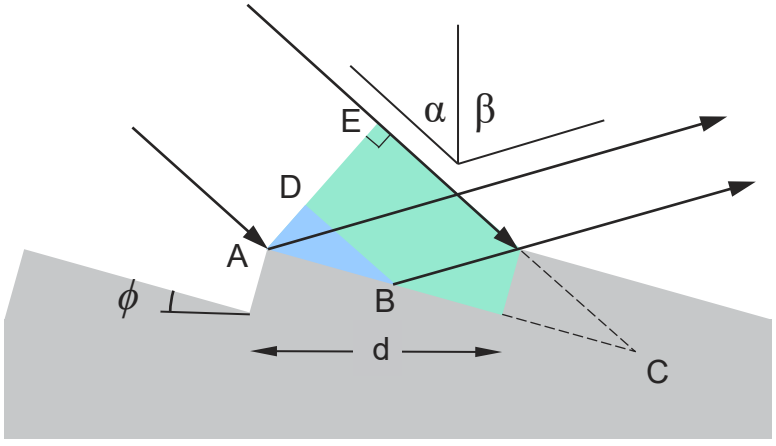

Fig. 11. Schematic of the blazed grating groove illumination and self shadowing. Only the non-shadowed part (AB) of the blazed facets contributes to diffraction effcieincy of the blazed order.

Averaging of the facet slope over the non-shadowed part of the blazed facets yields blaze angles of 2.55° and 2.70° for the 1st and 2nd order gratings respectively. Both angles are somewhat

Optics EXPRESS

smaller than the goal angle of 2.9° but the 2nd order grating is closer to the goal Although the mismatch is larger for the 1st order grating the expected impact on the diffraction efficiency is about the same as for the 2nd order grating since the 1st order grating is less sensitive to the errors in the blaze angle as seen in Fig. 5.

The reduced quality of the grooves of the 1st order grating is caused mostly by imperfections of the mold observed in Fig. 7(a). Higher LER and uneven line width of the mold pattern were inherited from the nanoimprint resist and eventually transferred to the Cr hard mask, increasing the risk of over-etching during the following KOH step. To avoid the over-etch and collapse of the grooves the etching time was reduced by a factor of two compared to the optimal time of 20 min. As a result of this, the grooves were not fully developed, the blaze angle was smaller than expected, and the groove depth was insufficient for successful nub removal by the following isotropic etching, resulting in rounding of the groove ridge.

4. Absolute diffraction efficiency: measurements and simulations

The diffraction efficiency of the gold-coated gratings was measured at beamline 6.3.2 of the ALS. The measurements were taken at an incidence angle of 82° by detector scans performed at different photon energies in the range of 760-1020 eV. The measured efficiency of the 1st and 2nd order gratings versus the photon energy is shown in Fig. 12 by lines with solid symbols. The theoretical efficiency calculated for an ideal sawtooth profile with a blaze angle of 2.9° is shown in Fig. 12 by lines with no symbols. An efficiency of 2.1% was measured for the 1st order grating at the energy of 850 eV (line with solid symbols in Fig. 12(a)). The experimental efficiency is substantially lower than the theoretical efficiency of 3.5% (line with no symbols in Fig. 12(a)). The 2nd order grating exhibits diffraction efficiency of 2.5% which is much closer to the theoretical value of 3.0%. Although the theoretical efficiency is higher for the 1st order grating, the experimental efficiency is higher for the 2nd order grating owing to the higher quality of the grating grooves.

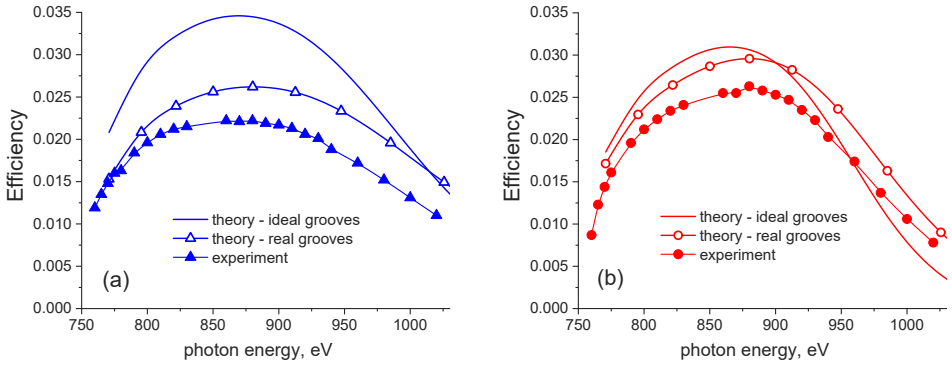

Fig. 12. Diffaction efficiency of the 6000 line/mm (a) and 3000 lines/mm (b) gratings with Au coating: theoretical efficiency for ideal triangular grooves (lines with no symbols), theoretical effciency for AFM measured groove profiles (lines with open symbols), and experimentally measured diffraction effcieincy (lines with solid symbols).

To evaluate the impact of groove shape on diffraction efficiency we performed simulations for the groove profiles measured by AFM (see Fig. 10). The results of the simulations are shown in Fig. 10 by lines with open symbols. Plugging-in the realistic groove profile results in significant reduction of efficiency for the 1st order grating as compared to the one with ideal groove shape (Fig. 12(a)). In contrast, the diffraction efficiency of the 2nd order grating with the realistic groove profile is close to the efficiency of an ideal grating (Fig. 12(b)). Both realistic simulations yield

Optics EXPRESS

efficiency which is somewhat higher than the experimental one due to surface roughness, LER and other minor defects of the gratings, which were not accounted in the simulations.

The results of simulations indicate that reduction of the efficiency for the 1st order grating is mainly caused by groove profile imperfections. To approach the theoretical diffraction efficiency, the fabrication process should provide flatness of the blazed facets, sharpness of the groove ridge, and steep slope of the anti-blazed facets. Although anisotropic wet etching can provide almost ideal triangular grooves, the final quality of the groove profile depends on all manufacture steps. For example, higher line edge roughness of the mold correlates with imperfections of groove profile for the 6000 lines/mm grating while a better mold results in almost ideal grooves for the 3000 lines/mm grating and higher diffraction efficiency.

5. Summary

We developed a process for fabrication of high groove density gratings for high resolution x-ray spectroscopy. Two full-sized blazed x-ray gratings with groove density of 3000 and 6000 lines/mm were fabricated for the new RIXS spectrometer of the Qerlin beamline which is currently under construction at the ALS. Diffraction efficiency of 2.5% was achieved for the 2nd order grating, close to that predicted by theory. Although 1st order gratings with higher groove density are preferable, they are significantly more challenging to make. Further refinement of the fabrication process is expected to yield improvement of the quality of the high groove density gratings and a commensurate increase in diffraction efficiency. However, the use of 2nd order gratings provides a robust way to obtain the performance we need and this use of higher order gratings points to many new possible applications in very high resolution soft x-ray spectroscopy.

Acknowledgments. The Advanced Light Source and the Molecular Foundry are supported by the Director, Office of Science, Office of Basic Energy Sciences, of the U.S. Department of Energy under Contract No. DE-AC02-05CH11231.

Disclosures. The authors declare no conflicts of interest.

This document was prepared as an account of work sponsored by the United States Government. While this document is believed to contain correct information, neither the United States Government nor any agency thereof, nor The Regents of the University of California, nor any of their employees, makes any warranty, express or implied, or assumes any legal responsibility for the accuracy, completeness, or usefulness of any information, apparatus, product, or process disclosed, or represents that its use would not infringe privately owned rights. Reference herein to any specific commercial product, process, or service by its trade name, trademark, manufacturer, or otherwise, does not necessarily constitute or imply its endorsement, recommendation, or favoring by the United States Government or any agency thereof, or The Regents of the University of California. The views and opinions of authors expressed herein do not necessarily state or reflect those of the United States Government or any agency thereof or The Regents of the University of California

Data availability. Data underlying the results presented in this paper are not publicly available at this time but may be obtained from the authors upon reasonable request.

References

1. L. J. P. Ament, M. van Veenendaal, T. P. Devereaux, J. P. Hill, and J. van den Brink, "Resonant inelastic x-ray scattering studies of elementary excitations," Rev. Mod. Phys. **83**(2), 705–767 (2011).
2. https://www.esrf.fr/home/UsersAndScience/Experiments/EMD/ID32/RIXS.html
3. I. Jarrige, V. Bisogni, Y. Zhu, W. Leonhardt, and J. Dvorak, "Paving the way to ultra-high-resolution Resonant Inelastic X-ray Scattering with the SIX beamline at NSLS-II," Synchrotron radiation news **31**(2), 7–13 (2018).
4. D. Cocco, G. Cutler, M. Sanchez del Rio, L. Rebuffi, X. Shi, and K. Yamauchi, "Wavefront preserving X-ray optics for Synchrotron and Free Electron Laser photon beam transport systems," Phys. Reports **974**, 1–40 (2022).
5. J. Gao, P. Chen, L. Wu, B. Yu, and L. Qian, "A review on fabrication of blazed gratings," J. Phys. D: Appl. Phys. **54**(31), 313001 (2021).
6. A. Sokolov, Q. Huang, F. Senf, J. Feng, S. Lemke, S. Alimov, J. Knedel, Th. Zeschke, O. Kutz, T. Seliger, G. Gwalt, F. Schäfers, F. Siewert, I. V. Kozhevnikov, R. Qi, Zh. Zhang, W. Li, and Zh. Wang, "Optimized highly efficient multilayer-coated blazed gratings for the tender X-ray region," Opt. Express **27**(12), 16833–16846 (2019).
7. Y. Fujii, K. I. Aoyama, and J. I. Minowa, "Optical demultiplexer using a silicon echelette grating," IEEE J. Quantum Electron. **16**(2), 165–169 (1980).
8. P. Philippe, S. Valette, O. Mata Mendez, and D. Maystre, "Wavelength demultiplexer: using echelette gratings on silicon substrate," Appl. Opt. **24**(7), 1006–1011 (1985).
9. D. L. Voronov, S. Park, E. M. Gullikson, F. Salmassi, and H. A. Padmore, "Highly efficient ultra-low blaze angle multilayer grating," Opt. Express **29**(11), 16676–16685 (2021).

Optics EXPRESS

10. D. L. Voronov, F. Salmassi, J. Meyer-Ilse, E. M. Gullikson, T. Warwick, and H. A. Padmore, "Refraction effects in soft x-ray Multilayer Blazed Gratings," Opt. Express **24**(11), 11334–11344 (2016).
11. D. L. Voronov, P. Lum, P. Naulleau, E. M. Gullikson, A. V. Fedorov, and H. A. Padmore, "X-ray diffraction gratings: precise control of ultra-low blaze angle via anisotropic wet etch," Appl. Phys. Lett. **109**(4), 043112 (2016).
12. D. L. Voronov, E.M. Gullikson, F. Salmassi, T. Warwick, and H.A. Padmore, "Enhancement of diffraction efficiency via higher order operation of a multilayer blazed grating," Opt. Lett. **39**(11), 3157–3160 (2014).
13. D. L. Voronov, E. H. Anderson, R. Cambie, S. Cabrini, S. D. Dhuey, L. I. Goray, E. M. Gullikson, F. Salmassi, T. Warwick, V. V. Yashchuk, and H. A. Padmore, "A 10,000 groove/mm multilayer coated grating for EUV spectroscopy," Opt. Express **19**(7), 6320–6325 (2011).
14. T. Warwick, Y.-D. Chuang, D. L. Voronov, and H. A. Padmore, "A multiplexed high resolution imaging spectrometer for resonant inelastic soft x-ray scattering spectroscopy," J. Synchrotron Radiat. **21**(4), 736–743 (2014).
15. J. H. Underwood and J. A. Koch, "High-resolution tunable spectrograph for x-ray laser linewidth measurements with a plane varied-line-spacing grating," Appl. Opt. **36**(21), 4913–4921 (1997).
16. https://www.pcgrate.com/
17. D. L. Voronov, E. M. Gullikson, and H. A. Padmore, "Large area nanoimprint enables ultra-precise x-ray gratings," Opt. Express **25**(19), 23334–23342 (2017).
18. N. Pala and M. Karabiyik, "Electron Beam Lithography (EBL)," in B. Bhushan, ed., *Encyclopedia of Nanotechnology* (Springer, 2012).
19. https://www.brukerafmprobes.com/p-3864-otespa-r3.aspx
20. A. P. Lukirskii and E. P. Savinov, "Use of diffraction gratings and echelettes in the ultrasoft x-ray region," Opt. Spectrosc. **14**, 147–151 (1963).
21. D. Maystre and R. Petit, "Some recent theoretical results for gratings: application for their use in the very far ultraviolet region," Nouv. Rev. Opt. **7**(3), 165–180 (1976).